Rough sea surface implications on receiver deghosting

Endrias Getachew Asgedom[1*], Okwudili Chuks Orji[1], Tilman Klüver[1], Hocine Tabti[1] and Walter Söllner[1]

Abstract

Efficient removal of ghost events is the key to achieving broadband seismic data. On the receiver-side, accurate ghost removal can be performed when both pressure and vertical particle velocity information is available. However, deghosting pressure-only measurements by spectral division with a flat sea surface or a statistical ghost function is still commonly applied. In this paper, we evaluate the performance of wavefield separation and deghosting with a flat sea surface (or statistical) ghost function for a rough weather marine seismic data acquisition. The behaviour of the pressure ghost function under rough sea conditions is analysed in comparison to the flat and the statistical pressure ghost functions. The three pressure ghost functions (i.e., true, flat, and statistical) converge to the same amplitude and phase values for the lower frequencies, but they diverge from each other for higher frequencies. The error created by wavefield separation and deghosting by spectral division is quantified, using synthetic and real seismic data. Wavefield separation provides deterministic and full receiver-side deghosted up-going wavefields, while both flat and statistical deghosting methods result in significant errors with implications in pre- and post-stack evaluation.

Introduction

The ultimate goal of marine seismic exploration is to deliver the true seismic response of the subsurface. This is only possible if seismic data with sufficient frequency bandwidth are acquired and faithfully processed. Broadband seismic data contain an adequate combination of low and high frequency information about the subsurface. The lower frequencies allow for structural imaging of deep targets whereas higher frequencies provide higher resolution. However, data acquisition and processing constraints can compromise the usable seismic bandwidth. During data acquisition, the presence of source- and receiver-side ghosts (i.e., reflections from the sea surface) significantly reduces the usable frequency band of the data by introducing notches in the amplitude spectra. The location and strength of these notches depends on the shape of the sea surface, the propagation speed of the seismic wave in water, the propagation direction, and the respective depths of the seismic sources and receivers. Over the years, the marine seismic industry has dedicated a lot of resources towards eradicating the unwanted effects of seismic ghosts.

In general, deghosting methods (or removal of ghost) are either processing-based or acquisition-based. In the processing-based method, only the pressure wavefield is recorded and a ghost function is constructed, describing the effects of the sea surface on the data, then deghosting is performed by spectral division, recursive filtering or integral inversion (Lindsey, 1960; Amundsen, 1993; Robinson and Treitel, 2008). This method of deghosting also includes the utilization of variable-depth (pressure-only) streamers which create diversity of notches to stabilize the deghosting process (Soubaras and Dowle, 2010), and the over/under streamer acquisition with appropriate deghosting strategies (Posthumus,1993; Özdemir et al., 2008; Kragh et al., 2010). In the acquisition-based method, we record pressure and particle velocity (or acceleration) and utilize the complementary nature of the ghosts of the two sensors in order to decompose the pressure wavefield into up- and down-going parts (Tenghamn et al., 2007; Caprioli et al., 2012). In this paper, we focus on rough sea surface receiver-side deghosting and analyse the differences between deghosting by spectral division and wavefield separation.

To understand the effects of rough sea surfaces on receiver-side ghost functions, we analyse the behaviour of the true ghost function in comparison to flat sea surface and statistical ghost functions. The true ghost function describes the true effects of the sea surface – which is time variable and contains effects of both coherent and incoherent scattering. In conventional data acquisition where only the pressure wavefield is recorded, assumptions about the sea surface are imposed in order to construct the ghost function. Two common assumptions are: the sea surface is flat and the sea surface height variation follows a Gaussian distribution. The former results in a ghost function computed with flat sea surface while the latter results in a ghost function computed with a statistical parameter describing the sea-surface state (e.g., standard deviation). Common between the two ghost functions is that they use a time invariant sea state and assume that sea surface scattering contributes only coherently with a given reflection coefficient. These ghost

[1] PGS

[*] Corresponding author, E-mail: endrias.asgedom@pgs.com

DOI: 10.3997/1365-2397.2017010

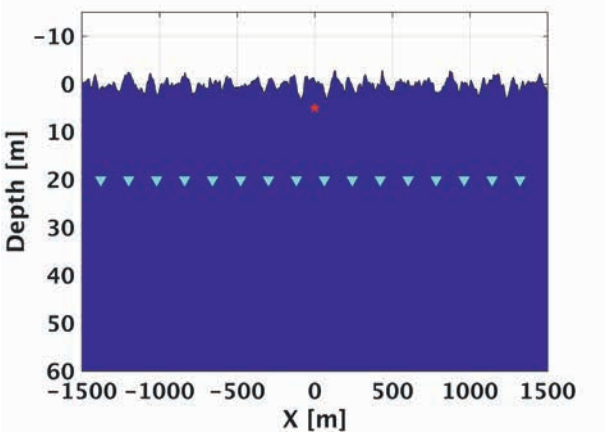

Figure 1 Acquisition geometry used to generate a synthetic shot gather.

functions may suffice at very low frequencies but lead to errors as frequency increases. We will demonstrate the detrimental effects of deghosting by spectral division using flat sea surface and statistical ghost functions in comparison to wavefield separation. The effects will be shown for both pre- and post-stack data.

Method

We consider a marine data acquisition configuration with sources at $r_s = (x_s, z_s)$ and receivers at $r_r = (x_r, z_r > z_s)$. When both pressure and vertical particle velocity data are available at the streamer, using acoustic reciprocity, it is possible to show that the total pressure wavefield can be decomposed into up- and down-going wavefields (Fokkema and van den Berg, 1993). This receiver-side wavefield separation may be written in the frequency-wavenumber domain as (Day et al., 2013)

$$P_{up}^{ws}\left(\omega,k_x\,|\,z_r\right)=\frac{1}{2}\left[P\left(\omega,k_x|z_r\right)-\frac{\omega\rho}{k_z}V_z\left(\omega,k_x\,|\,z_r\right)\right], \quad (1)$$

where, $P_{up}^{ws}(\omega,k_x|z_r)$, $P(\omega,k_x|z_r)$ and $V_z(\omega,k_x|z_r)$ represent respectively the wavefield separated up-going pressure, the total pressure, and the total vertical particle velocity wavefields at angular frequency ω, horizontal wavenumber k_x and receiver depth z_r. The scaling factor $\frac{\omega\rho}{k_z}$ contains the acoustic impedance and the obliquity correction needed to convert vertical particle velocity into pressure. Here, ρ and k_z are the mass density at the receiver location and the vertical wavenumber, respectively. The scaling factor requires stabilization at 90° emergence angle – as a result of the zero value of k_z at this angle. Practically, this may be avoided by including exponential damping on both input data p and v_z and then adding the equivalent imaginary number in the temporal frequency axis of the scaling factor. The exponential damping on the data is removed after the wavefield separation process.

The effects of the sea surface on the receiver-recording can be described using the ghost function. The true ghost function $G_p^{true}\left(\omega,k_x\,|\,z_r\right)$ of a given data can be extracted from the recorded total and up-going pressure wavefields as

$$G_p^{true}\left(\omega,k_x\,|\,z_r\right)=\frac{P\left(\omega,k_x\,|\,z_r\right)}{P_{up}\left(\omega,k_x\,|\,z_r\right)}\ . \quad (2)$$

It is pertinent to note that the true ghost function requires knowledge of the up-going wavefield, which can only be obtained through proper wavefield separation. The true ghost function is unknown for conventional marine data acquisitions where only the pressure wavefield is acquired. Thus, in deghosting pressure-only data, the sea surface is assumed to be flat with a reflection coefficient of R_{flat} and the true ghost function is approximated with a flat sea surface ghost function given by

$$G_p^{flat}\left(\omega,k_x|z_r\right)=1+R_{flat}\exp\left(-2ik_z z_r\right) \quad (3)$$

In practice, we set $0 > R_{flat} \geq -1$. This approximation is crude and simplistic since it does not take the sea surface height variation into account. In addition it has close to zero values at the notch locations which results in instabilities when used for deghosting. To relax this constraint, a more refined statistical ghost function can be defined, which assumes that the sea surface height variation follows a Gaussian distribution with zero mean and variance of σ^2. The statistical ghost function is the result of the expectation of the true ghost function and it is given by

$$G_p^{stat}\left(\omega,k_x\,|\,z_r\right)=\left\langle G_p^{true}\left(\omega,k_x\,|\,z_r\right)\right\rangle=1+R_{stat}\left(\omega,k_x\right)exp\left(-2ik_z z_r\right), \quad (4)$$

where <[]> denotes the expectation operator and $R_{stat}(\omega,k_x)=-\exp(-2(k_z\sigma)^2)$ is the coherent sea surface reflection coefficient – which is angle and frequency dependent (Ogilvy, 1987; Orji et al., 2013).

Receiver-side deghosting can be performed by spectrally dividing the recorded pressure field with that of a given ghost function (Amundsen, 1993). Flat sea surface and statistical ghost functions are the two commonly used ghost functions. However, both ghost functions have zeros (e.g., at 90° emergence angle and notch locations for the flat sea surface ghost function and at 90° emergence angle for the statistical ghost function) and therefore require stabilization during the deghosting process.

Synthetic data examples

Two dimensional (2D) marine seismic data are generated using the Kirchhoff method (Thorsos, 1987; Laws and Kragh, 2002; Orji et al., 2011) from a 2D model consisting of a one dimensional (1D) rough sea surface, using a Pierson-Moskowitz spectrum (Pierson and Moskowitz, 1964), and a flat sea floor reflector at a depth of 500 m (cf. Figure 1). The sea surface has a significant wave height of 4.6 m, which is a very rough sea surface but still within the capabilities of current marine seismic acquisition. The sources and receivers are located at a depth of 5 m and 20 m, respectively. The cable length is 6 km with 3 m receiver spacing. A total of 250 shots were generated at intervals of 3 m. The dense spatial sampling has been chosen in order to avoid spatial aliasing. Each receiver comprises of collocated pressure and vertical particle velocity single sensors. Figure 2 shows the computed data in TX (time-space) and FK (frequency-wavenumber) domains. Figures 2a-2c show respectively a shot gather of the modelled total, up- and down-going pressure wavefields in the TX domain. The corresponding FK domain plots are shown in Figures 2d-2f. For plotting purposes, all data have been multiplied with $\sqrt{i\omega}$ to remove the 2D frequency response of the data. In addition, all FK domain plots are shown within the signal cone.

Here, for simplicity, source side ghost, direct wave and surface related multiples are not considered. Thus, the modelled

up-going pressure wavefield is characterized both by smoothly varying amplitude in TX (cf. Figure 2b) and a smooth spectrum in FK (cf. Figure 2e). On the other hand, the down-going wavefield contains reflections from the rough sea surface that introduces both coherent scattering (or the mean field related to the smooth part of the sea surface) and incoherent scattering (or the diffuse field related to the rough part of the sea surface) that result in fluctuations in the wavefield – this is visible both in TX and FK domains (cf. Figures 2c and 2f). The total pressure wavefield is the superposition of the up-going and the down-going wavefields (cf. Figure 2a) resulting in destructive and constructive interference. Since the sea surface is rough, this manifests itself in the frequency domain as diversity of notch structures (i.e., locations where destructive interference occurs, cf. Figure 2d).

Considering a shot record, the modelled total and up-going pressure wavefields are used to compute the true ghost function based on Equation (2). The amplitude spectrum of this ghost function is shown in Figure 3a. As expected, the spectrum of the true ghost function has a diversity of notches. Assuming the root-mean-square (RMS) height of the sea surface is known, we can approximate the true ghost function with the statistical ghost function. Figure 3b shows the amplitude spectrum of the statistical ghost function computed using Equation (4) where the RMS height of the sea surface, computed from the significant wave height of the sea surface (Carter et al., 1986; Laws and Kragh, 2002), is 1.15 m. In Figure 3b the notches are periodic with frequency – the periodicity is dictated by the receiver depth (i.e., the distance from a sea surface with zero mean wave height). The statistical reflection coefficient R_{stat} has a maximum absolute value of 1 and decreases

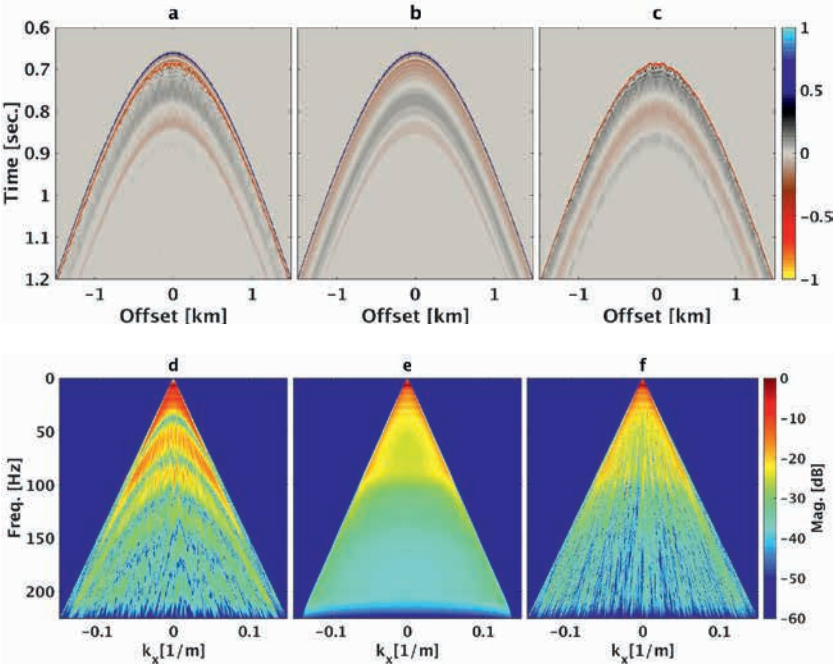

Figure 2 Modelled shot gather data in time-space: total pressure (a), up-going pressure (b), and down-going pressure (c). The corresponding amplitude spectra in FK domain are shown respectively for the total, up-going and down-going pressure in (d), (e), and (f).

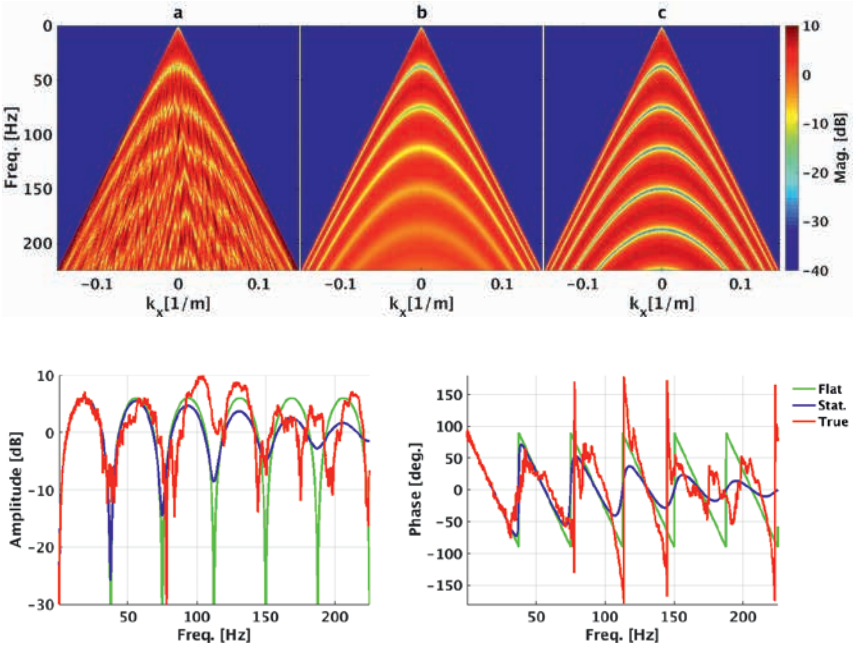

Figure 3 Amplitude spectra of the ghost functions: true (a), statistical (b), and flat sea surface (c). The amplitude and the phase of all three ghost functions at vertical emergence angle are shown respectively in (d) and (e). Here the true, statistical, and flat sea surface ghost functions are shown in red, blue, and green, respectively.

exponentially with frequency. However, the reflection coefficient is also angle dependent – as the emergence angle increases from 0°, R_{stat} tends to the absolute value of 1 as the angle approaches 90° (e.g., Orji et al., 2013). Thus, in Figure 3b the spectral depth of the notches decreases with increasing frequency and increases with increasing emergence angle. One consequence of a large reflection coefficient on the statistical ghost function is the sharp change in phase – this is apparent for notch locations at lower frequencies (cf. Figure 3e) and higher emergent angles.

If the sea surface shape information is unavailable, the sea surface shape may be approximated with a flat surface and one can perform deghosting using the flat sea surface ghost function. The amplitude spectrum of the flat sea surface ghost function computed using Equation (3) is shown in Figure 3c. Similar to the statistical ghost spectrum, the notches are periodic. Nevertheless, the spectrum at the notches show equal strength for all angles and frequencies in contrast to the statistical ghost spectrum. The amplitude spectra of the flat sea surface and the statistical ghost functions are smooth. This is because both ghost functions represent only the coherently scattered energy from flat sea and rough sea surfaces, respectively. This is in contrast to the true ghost function amplitude spectrum. In addition, note that the difference at the notches between the true ghost function and flat and statistical ghost functions increases with frequency. At lower frequencies, all three ghost functions converge to the same amplitude and phase values. This is demonstrated in Figures 3d and 3e which show respectively, the amplitude and the phase spectra of the three ghost functions at vertical emergence angle.

In the absence of noise and numerical instabilities, deghosting via spectral division using the true ghost function can be shown to give perfect results (accurate up-going wavefield). In this work, the focus is to compare wavefield separation results with deghosting based on spectral division – using flat sea and statistical ghost functions. Wavefield separation was applied based on Equation (1) using the modelled total pressure and vertical particle velocity data. The resulting up-going wavefield is compared with results from the flat sea surface and the statistical deghosting in the pre-stack domain. Figure 3a shows the up-going pressure wavefield after wavefield separation. A comparison of the modelled and separated up-going wavefields (Figure 2b and 4a) show a very good match. Deghosting by the spectral division of the modelled total pressure with the statistical and the flat sea surface ghost functions is then performed and the results in the TX domain are shown in Figure 4b and 4c, respectively. Comparison of these results with the modelled up-going wavefield shows a poor match. The results from both the statistical and the flat sea surface deghosting have residual scattered down-going energy remaining in the deghosted data. In addition, the two deghosting results have 'ringing' events that compromise the temporal resolution of the main reflection event. This effect is more pronounced in the flat sea surface deghosting result relative to the statistical counterpart. The ringing feature is caused by deghosting with a ghost function that has a sharp phase change at the notches – which is different from the phase of the true ghost function.

In order to estimate the error associated with each method, we computed the relative error between the modelled up-going wavefield and each of the up-going wavefields obtained from the three different approaches above. Figures 4d-f show the quantified relative errors in the FK domain. The relative error from the wavefield separation result is zero everywhere except at the edges of the signal cone (Figure 4d). This error is caused mainly because the modelled up-going wavefield does not have energy at angles close to 90°, resulting in an unstable computed relative error. The results from both the statistical and the flat sea surface deghosting (respectively Figure 4e and 4f) show significant errors mainly owing to unaccounted coherent and incoherent energy. Observe that these errors increase with frequency. The flat sea surface deghosting result exhibits strong errors close to the notches which can also be seen in the statistical deghosting result at lower frequency notches (e.g., the second and third notches), where the

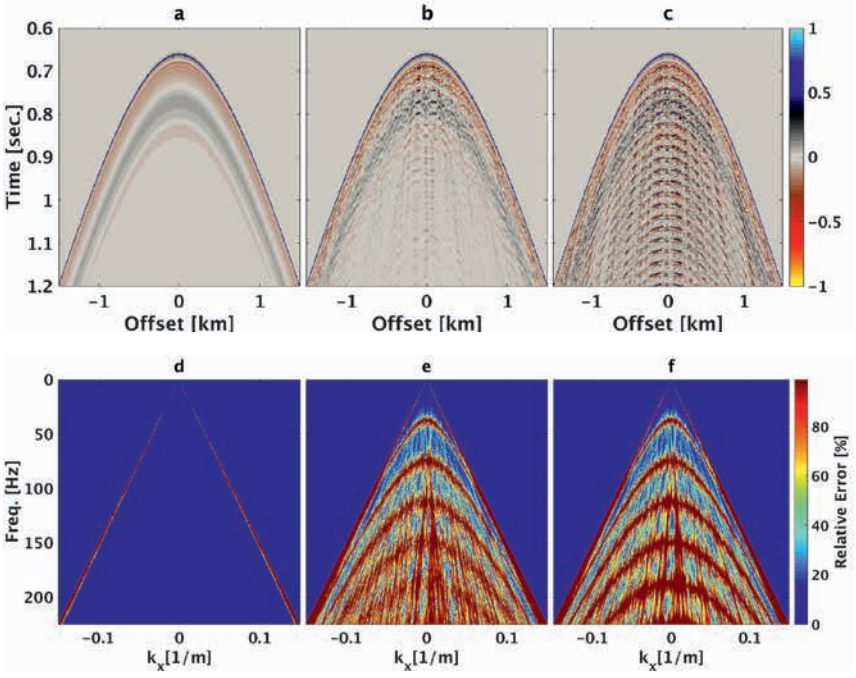

Figure 4 Up-going pressure wavefield obtained by performing wavefield separation (a), statistical deghosting (b), and flat sea surface deghosting (c). Relative errors of wavefield separation (d), statistical deghosting (e), and flat sea surface deghosting (f).

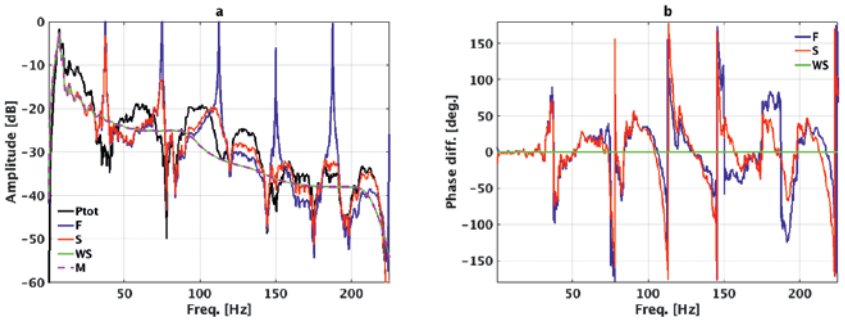

Figure 5 Amplitude spectra: flat sea surface deghosted up-going wavefield (F), statistical deghosted up-going wavefield (S), wavefield separated up-going wavefield (WS), modelled up-going wavefield (M), and the total pressure wavefield (Ptot) is shown in (a). The phase difference between the modelled and wavefield separated and deghosting results is shown in (b).

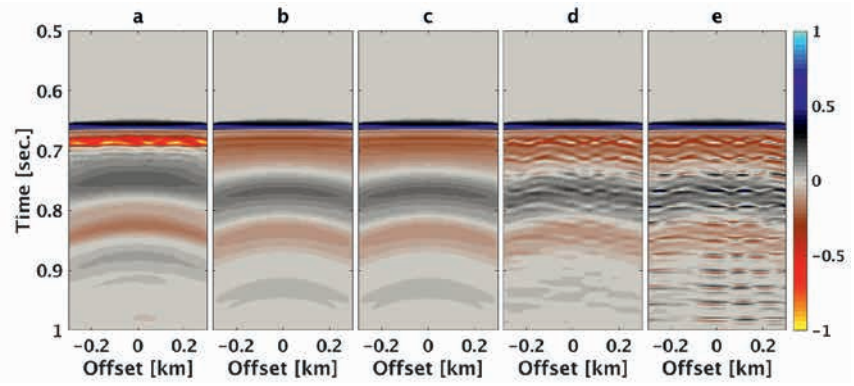

Figure 6 CIGs representing the total pressure (a), modelled up-going pressure (b), wavefield separated up-going pressure (c), statistically deghosted up-going pressure (d) and flat sea surface deghosted up-going pressure (e).

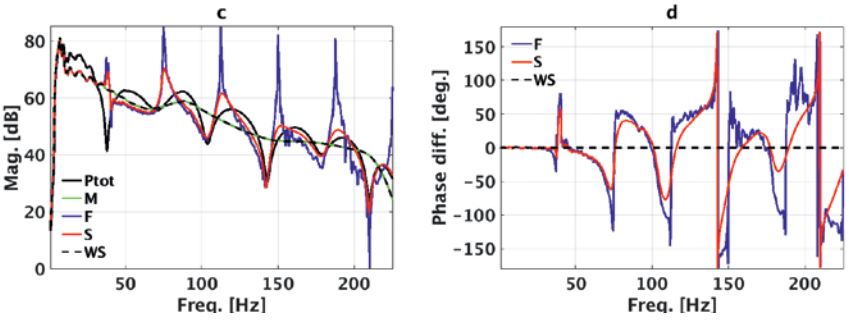

Figure 7 Amplitude spectra of a trace in a CIG: flat sea surface deghosted up-going wavefield (F), statistically deghosted up-going wavefield (S), wavefield separated up-going wavefield (WS), modelled up-going wavefield (M), and the total pressure wavefield (Ptot) is shown in (a). The phase difference between the modelled and wavefield separated and deghosting results is shown in (b).

notches are deep and have sharp phase changes. Moreover, the convergence of the three methods towards the lower frequencies is pertinent to note.

To demonstrate the similarity between the results of wavefield separation and deghosting at lower frequencies, we plot the amplitude spectra of the modelled up-going wavefields and computed counterparts based on wavefield separation and deghosting by spectral division (i.e., flat sea surface and statistical deghosting). Figure 5a shows the plot at the vertical emergence angle. The phase difference between the results of wavefield separation and deghosting by spectral division relative to the modelled up-going wavefield at the vertical emergence angle is also shown in Figure 5b. Observe firstly that the notch frequencies of the total pressure data does not correspond to the frequencies where deghosting by spectral division (i.e., flat sea surface and statistical) have their largest errors. This effect is more pronounced at higher frequencies. These differences arise because the total pressure data is from a rough sea surface with constant receiver depth while the up-going results from spectral division are from a flat sea surface and constant receiver depth. Secondly, as expected both the flat sea surface and statistical deghosting results have significantly smaller differences in comparison with the modelled up-going wavefield towards the lower frequencies. In practice, motion sensors used to acquire the vertical particle velocity (or acceleration) data in multi-component towed streamer acquisitions are often contaminated with vibration noise at the lower frequencies. Nevertheless, given the convergence between the results from wavefield separation and the results from deghosting by spectral division at lower frequencies, wavefield separation at the lower frequency end can be replaced by the flat sea surface (or the statistical) deghosting.

In the pre-stack domain, a convenient way of reducing the effects of the rough sea surface is to perform pre-stack migration and analyse the data in Common Image Gathers (CIGs). Thus, we now illustrate and evaluate the errors created by wavefield separation and deghosting in the pre-stack domain using CIGs. To generate the CIGs, we migrate the wavefield separated up-going wavefield and the counterparts obtained by spectral division deghosting offset-by-offset using a Kirchhoff-type pre-stack migration algorithm. Figures 6a-e show the CIG of the total, the modelled up-going, the wavefield separated up-going, the statistically deghosted up-going and the flat sea surface deghosted up-going pressure data, respectively. The wavefield separation result shows a near perfect match in comparison with the result from the modelled up-going wavefield. Although the statistically

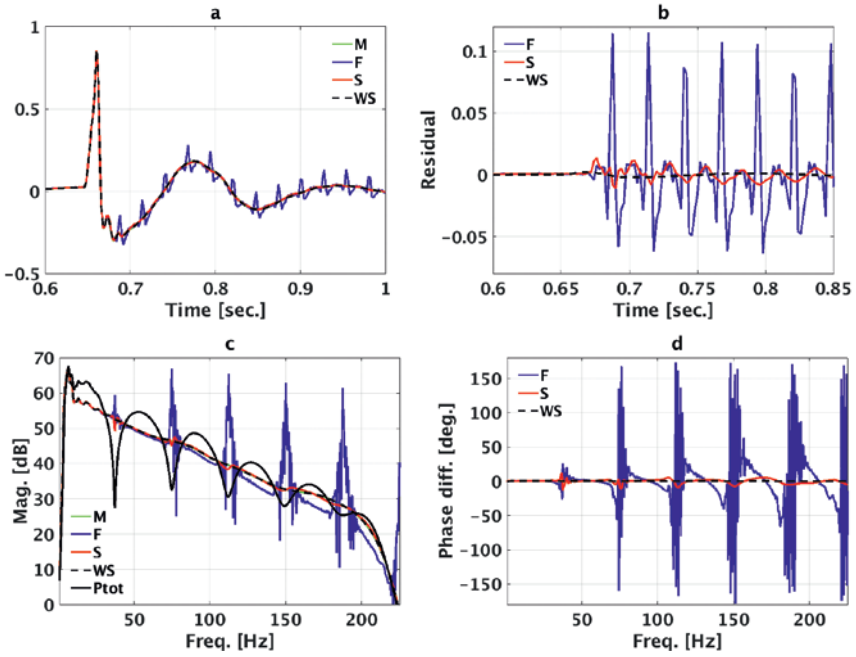

Figure 8 Time migrated traces modelled up-going pressure (M), wavefield separated up-going pressure (WS), statistically deghosted up-going pressure (S), flat sea surface deghosted up-going pressure (F), and the total pressure (Ptot) are shown in (a). Residual between modelled and wavefield separated/deghosted results (b). Amplitude spectra of modelled and wavefield separated/deghosted results (c). Phase difference between modelled and wavefield separated/deghosted results (d).

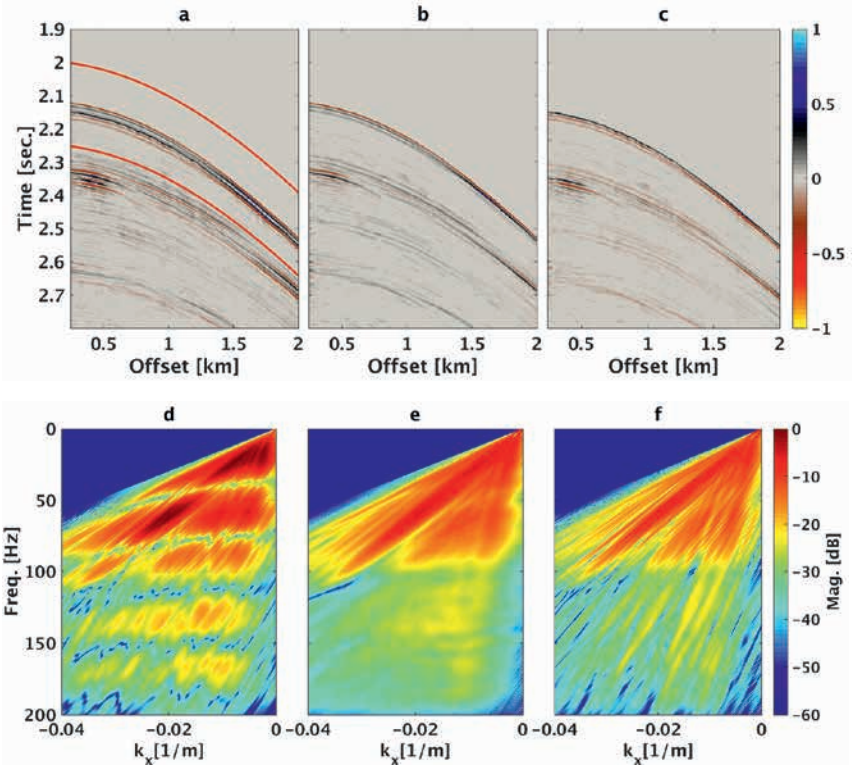

Figure 9 Total (a), up-going (b), and down-going (c) pressure wavefields in time-space. The corresponding amplitude spectra in the FK domain are shown respectively for the total, up-going, and down-going pressure in (d), (e) and (f).

deghosted result shows a good match at the main up-going energy, it still has considerable residual down-going energy (cf. Figure 6d). As expected, this effect is even more pronounced in the result from the flat sea surface deghosting which has a significant residual down-going energy and ringing feature (related to the sharp phase change of the ghost function) in the data. In general, pre-stack migration of the data has reduced the fluctuation effects of the rough sea surface scattering. This is shown in Figures 7a and 7b where we plot the amplitude spectra and phase difference (relative to the modelled up-going wavefield) of the data in a CIG. Here, it is pertinent to note that the amplitude spectrum of the total pressure after pre-stack migration is smoother compared to the total pressure before migration (compare Figures 5a and 7a). Furthermore, the notch frequencies of the total pressure data correspond better to the frequencies where deghosting by spectral division has its largest errors. However, as demonstrated, pre-stack migration cannot completely compensate for the sea surface effects.

Finally, the CIG data can be stacked to simulate the time-migrated image of the subsurface. In this domain, we analyse the results of the up-going pressure data obtained from wavefield separation and the spectral division deghosting results. These are then

compared to the image obtained from the modelled up-going pressure wavefield. After stacking the data in the CIGs, the results are shown in Figures 8a-d. Figure 8a show the stacked traces (or time migrated images) while the corresponding residual (relative to the result of the modelled up-going pressure wavefield) is shown in Figure 8b. As expected, wavefield separation gives in this case an excellent result with nearly zero residual while the statistical and flat sea surface deghosting results have residuals after the main peak of the signal. Figure 8c shows the amplitude spectrum of the stacked traces while the corresponding phase difference relative to the result from modelled up-going pressure data is shown in Figure 8d. The wavefield separated result matches perfectly with the modelled up-going pressure result both in amplitude and phase. On the other hand, the statistical deghosting result has its main source of amplitude and phase error at the second pressure notch of the ghost function while flat sea surface deghosting has both amplitude and phase errors at all the notch frequencies (including the vicinity) of the ghost function except the notch at zero Hertz. It is important to note here that the amplitude spectrum of the total pressure is smooth (compare Figure 8c with 5a) and the depth of the notches reduces with increasing frequency. Moreover, the flat sea surface and the statistical deghosting results deviate from the modelled up-going pressure results at the notch frequencies of the total pressure result (compare Figure 8c with 5a).

Field data example

The field data were acquired offshore the Falkland Islands with collocated pressure and vertical particle velocity sensors which enabled a full receiver-side separation of the total pressure wavefield into its up-going and down-going parts. Statistical and flat sea surface deghosting were also applied to the data and the results evaluated in comparison to the wavefield separation result. As demonstrated in the previous section the methods converge at lower frequencies. Thus, below 15 Hz (the vertical particle velocity sensor is susceptible to vibration noise at lower frequencies) the wavefield separation is replaced with flat sea surface deghosting. The total pressure wavefield, the separated up-going and the down-going pressure wavefields in the TX domain are shown in Figures 9a-c. Observe that the up-going and down-going wavefields have opposite polarity relative to each other. The

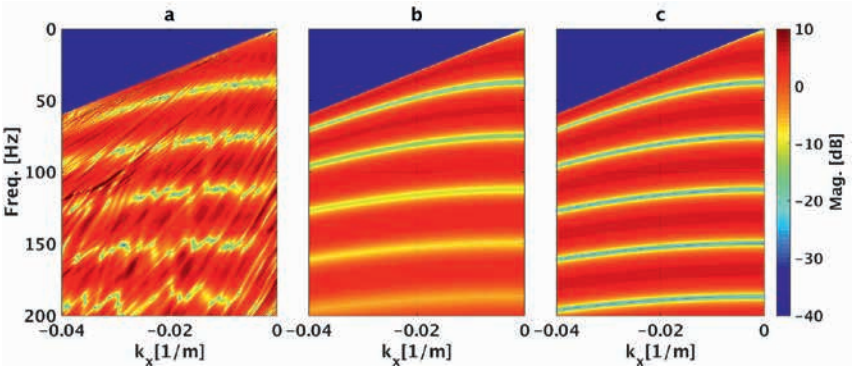

Figure 10 Amplitude spectra of the true (a), statistical (b) and flat sea surface (c) ghost functions.

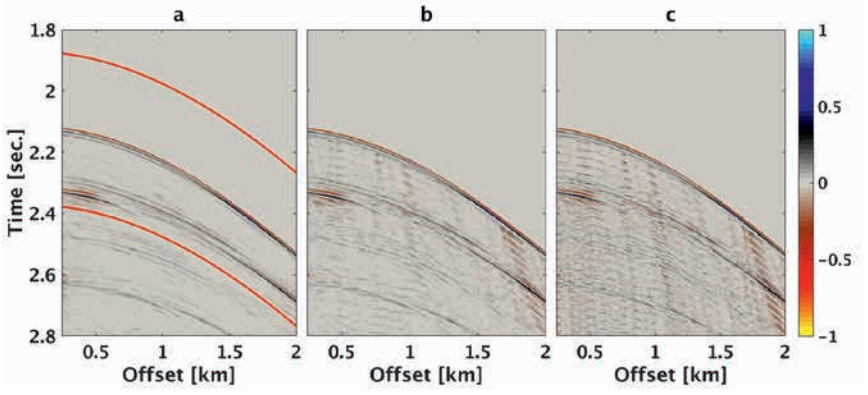

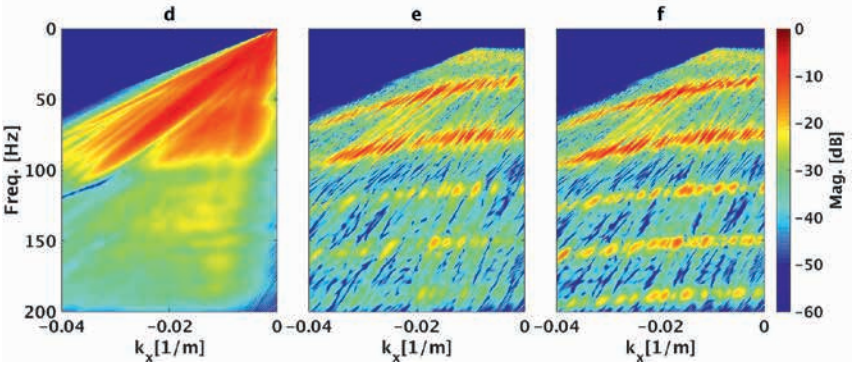

Figure 11 Up-going wavefield in time-space domain: Wavefield separated (a), statistically deghosted (b), and flat sea surface deghosted (c). Amplitude spectra of the wavefield separated (d), residual of the statistical (e) and flat sea surface (f) deghosted results.

corresponding FK domain spectra computed within the window indicated in Figure 9a are shown in Figures 9d-f. Similar to what is observed in the synthetic data, the total pressure wavefield contains a diversity of notches in the amplitude spectrum and the up-going wavefield is smooth both in the TX and FK domain (i.e., within the selected window the up-going wavefield does not see the sea surface). The observed undulation in the TX domain of the down-going wavefield is a result of the scattering of the wavefield at the sea surface, this scattered energy from the sea surface manifests itself as linear features in the FK domain (cf. Figure 9f).

To characterize the effects of the sea surface, we computed the true ghost function using the recorded total pressure and the wavefield separated up-going wavefield. The amplitude spectrum of this true ghost function for a given shot gather, within the window indicated in Figure 9a, is shown in Figure 10a where the rough sea surface imprint manifests itself as a diversity of notch locations. The statistical ghost function is computed by first coherently averaging the true ghost functions over 950 shots. Here, since field data is contaminated by acquisition noise unlike the synthetic data, we construct the statistical ghost function using Equation (4) by finding the optimal RMS height of the sea surface such that the constructed ghost function and that obtained by averaging are similar. The amplitude spectrum of this statistical ghost function is shown in Figure 10b. The second and third pressure ghost notches of the statistical ghost function are deep and this can create errors in the deghosting process. The flat sea surface ghost function is computed based on Equation (3) and its amplitude spectrum is shown in Figure 10c. It is important to state here that the statistical ghost function computed by coherent averaging of the true ghost function can only be obtained if the correctly separated up-going wavefields are available.

Pre-stack wavefield separation and deghosting results are analysed in shot gather and CIG domains. In the shot domain, the wavefield separation result – used as a reference – is shown in time-space in Figure 10a and in the FK domain (within a window shown in Figure 10a) in Figure 10d. The statistical and flat sea surface deghosted results in time-space are shown respectively in Figure 10b and c. Both deghosting results show remaining down-going wavefield and a ringing feature. At the locations of the lower frequency notches – except at zero Hertz – both deghosting methods blow up the noise in the data (i.e., at those notch locations where the signal-to-noise ratio in the total pressure data is poor). To

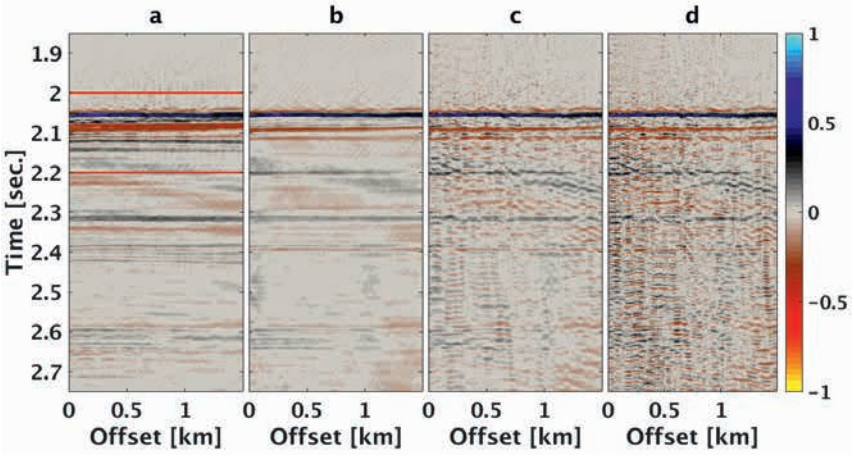

Figure 12 CIG for the total pressure (a), wavefield separated (b), statistically deghosted (c) and flat sea surface deghosted (d) up-going wavefields.

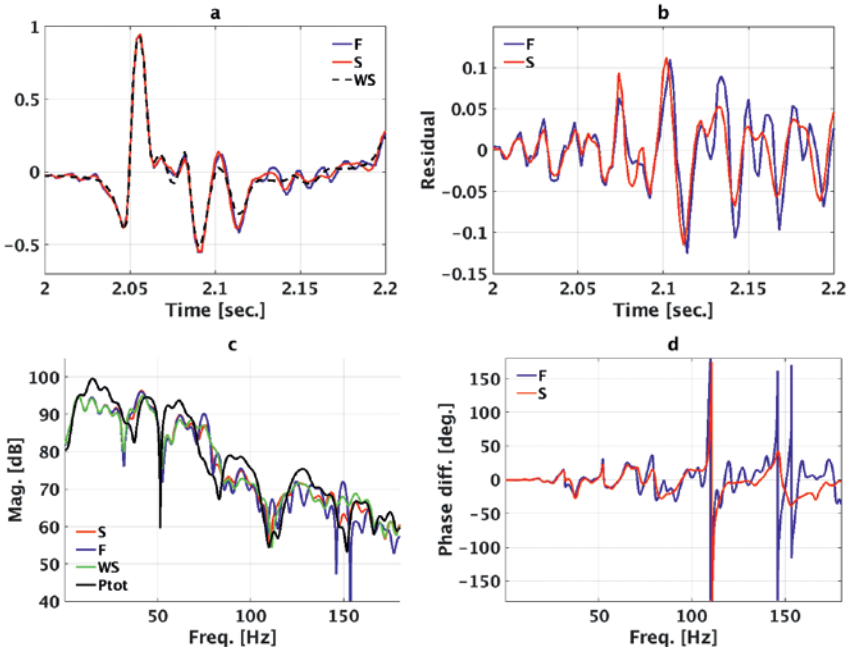

Figure 13 Stacked traces of total pressure (Ptot), wavefield separated (WS), statistically deghosted (S), and flat sea surface deghosted (F) up-going wavefields (d). Amplitude spectra of wavefield separated, statistically deghosted, and flat sea surface deghosted up-going wavefields (e).

quantify the difference between wavefield separation and that of the two deghosting methods, we computed the amplitude spectrum of the residual between wavefield separation and the two deghosting results. The statistical deghosting residual amplitude spectrum shows significant errors at the second and third pressure notch locations of the ghost function and also it shows significant error related to the sea surface for higher frequencies. The flat sea surface deghosting residual shows significant errors for all pressure notch locations of the ghost function.

To reduce the effects of the rough sea surface on pre-stack deghosted results, we performed pre-stack migration and analysed the results in CIGs. The CIG of the total pressure, the wavefield separated up-going wavefield, and the statistical and flat sea surface deghosted up-going wavefields are shown respectively in Figures 12a-e. The undulation created by the scattering at the sea surface is reduced in the CIG of the total pressure as a result of the pre-stack migration. Though, the undulation in the CIGs of the flat sea surface and statistically deghosted results are reduced, remaining residual down-going energy in both the results is clearly visible. A comparison of the wavefield separated up-going wavefield with that of the flat sea surface and statistically deghosted up-going wavefields demonstrate the superiority of wavefield separated CIGs for pre-stack geophysical analysis – e.g. Angle-Vs-Offset (AVO) analysis.

In order to analyse the post-stack differences between wavefield separation and deghosting, the data in the CIGs shown in Figure12 are stacked to generate the corresponding time-migrated images of the subsurface. Figure 13a shows the stacked traces of the wavefield separated up-going wavefield, and the flat sea surface and statistically deghosted up-going wavefields. The results of the two deghosting methods match that of the wavefield separation at the main peak of the sea floor reflector. For all events below the sea floor reflector, the deghosted results significantly differ from that of wavefield separation (cf. Figure 13b). Figures 13c and 13d show the amplitude spectra of the stacked traces of the three methods and the total pressure (selected within the window shown in Figure 12a) and the phase difference between the result of wavefield separation and deghosting, respectively. The deghosted results are similar to that from wavefield separation at lower frequencies as expected – for frequencies lower than 15 Hz, the wavefield separation is replaced by flat sea surface deghosting. Nevertheless, both of the deghosted results differ significantly from the wavefield separation result above 15 Hz. Moreover, the statistically deghosted result is more similar to the result from wavefield separation in comparison to that of the flat sea surface deghosting scheme, as expected.

Conclusion

Amplitude and phase preserving properties of wavefield separation and receiver side deghosting with flat or statistical sea surface assumption are analysed in both pre-stack (i.e., shot and CIG domains) and post-stack (i.e. time migrated image domain) using rough weather marine synthetic and field data examples. Wavefield separation, the wave theoretically correct solution, provides the correct up-going wavefield in both pre- and post-stack domains. Although the three solutions converge at lower frequencies to the correct solution, deghosting with a statistical ghost function creates significant errors at the second and third pressure notch locations. In addition, deghosting with a flat sea surface ghost function creates errors for all the higher pressure notch locations. Pre-stack deghosting results show scattering errors that increase with frequency while the post-stack deghosting results show errors that are mainly concentrated at the pressure notch locations.

Acknowledgements

The authors would like to thank PGS for permission to publish this work.

References

Amundsen, L. [1993]. Wavenumber-based filtering of marine point-source data. *Geophysics*, **58**, 1335-1348.

Caprioli, P., Özdemir, K., van Manen, D.J., Mahat, S., Özbek, A., Kragh, E. and Christie, P. [2012]. Combination of multi-component streamer pressure and vertical particle velocity – Theory and application to data. *82nd SEG Annual International Meeting*, Expanded Abstracts, 1-5.

Carter, D.J.T., Challenor, P.G., Ewing, J.A., Pitt, E.G., Srokosz, M.A. and Tucker, M.J. [1986]. *Estimating Wave Climate Parameters for Engineering Applications.* HMSO OTH. 86228.

Day, A., Klüver, T., Söllner, W., Tabti, H. and Carlson, D. [2013]. Wavefield-separation methods for dual-sensor towed-streamer data. *Geophysics*, **78**, WA55-WA70

Fokkema, J.T. and van den Berg, P.M. [1993]. *Seismic applications of acoustic reciprocity.* Elsevier Science Publishing Company.

Kragh, E., Muyzert, E., Curtis, T., Svendsen, M. and Kapadia, D. [2010]. Efficient Broadband Marine Acquisition and Processing for Improved Resolution and Deep Imaging. *The Leading Edge*, **29**, 464-469.

Laws, R and Kragh, E. [2002]. Rough seas and time-lapse seismic. *Geophysical Prospecting*, **50**, 195-208.

Lindsey, J.P. [1960]. Elimination of seismic ghost reflections by means of a linear filter. *Geophysics*, **25**, 130–140

Ogilvy, J.A. [1987]. Wave scattering from rough surfaces. *Rep. Prog. Phys*., **50**, 1553-1608.

Orji, O.C., Söllner, W. and Gelius, L.J. [2011]. Effects of time-varying sea surface in marine seismic data. *Geophysics*, **77**, 33-43

Orji, O.C., Söllner, W. and Gelius, L.J. [2013]. Sea surface reflection coefficient estimation. *83th SEG Annual Meeting,* Expanded Abstracts, SEG-2013-0944

Özdemir, A.K., Caprioli, P., Özbek, A., Kragh, E. and Robertsson, J.O.A. [2008]. Optimized deghosting of over/under towed-streamer data in the presence of noise. *The Leading Edge*, **27**, 190-199.

Pierson, W.J. and Moskowitz, I. [1964]. A proposed spectral form for fully developed wind seas based on the similarity theory of S. A. Kitaigorodskii. *Journal of Geophysical Research*, **69**, 5181-5190.

Posthumus, B.J. [1993]. Deghosting using a twin streamer configuration, *Geophysical Prospecting*, **41**, 267-286.

Robinson, E.A., and Treitel, S. [2008] *Digital imaging and deconvolution: The ABCs of seismic exploration and processing.* SEG.

Soubaras, R. and Dowle, R. [2010]. Variable-depth streamer – a broadband marine solution. *F*irst Break, 28, 89-96.

Tenghamn, S.T.L., Vaage, R.S. and Borresen, C. [2007]. A dual-sensor towed marine streamer: Its viable implementation and initial results. 77th SEG Annual International Meeting, Expanded Abstracts, 989–993.

Thorsos, E.I. [1987]. The validity of the Kirchhoff approximation for rough surface scattering using a Gaussian roughness spectrum. Journal of the Acoustical Society of America, 83, 78-92.